Title
Probing Ionomer Interactions with Electrocatalyst Particles in Solution

Journal
ACS Energy Letters, 6(6)

ISSN
2380-8195

Authors
Berlinger, Sarah A
McCloskey, Bryan D
Weber, Adam Z

Publication Date
2021-06-11

DOI
10.1021/acsenergylett.1c00866

Peer reviewed

Probing Ionomer Interactions with Electrocatalyst Particles in Solution

Sarah A. Berlinger[1,2], Bryan D. McCloskey[1,2], Adam Z. Weber[2,]*

[1]Department of Chemical and Biomolecular Engineering, University of California, Berkeley, Berkeley, CA 94720

[2]Energy Technologies Area, Lawrence Berkeley National Laboratory, Berkeley, CA 94720

Corresponding Author

*Adam Z. Weber: azweber@lbl.gov

ABSTRACT

The interaction between ionomer (ion-conducting polymer) and catalyst particles in porous electrodes of electrochemical energy-conversion devices is a critical yet poorly understood phenomenon that controls device performance: electrode morphology is controlled by ionomer/particle interactions in precursor inks during electrode formation. In this letter, we probe the origin of this interaction in inks to unravel the complexities of the ionomer/particle adsorption interactions. Quartz-crystal microbalance studies detail ionomer adsorption (with a range of charge densities) to model surfaces under a variety of solvent environments, and isothermal-titration-calorimetry experiments extract thermodynamic binding information to platinum- and carbon-black nanoparticles. Results reveal that under the conditions tested, ionomer binding to platinum is similar to carbon, suggesting that adsorption to platinum-on-carbon catalyst particles in inks is likely dictated mostly by entropic interactions with the carbon surface. Furthermore, water-rich solvents (relative to mixed water/propanol) promote ionomer adsorption. Finally, ionomer dispersions change with time, yielding dynamic binding interactions.

TOC GRAPHIC

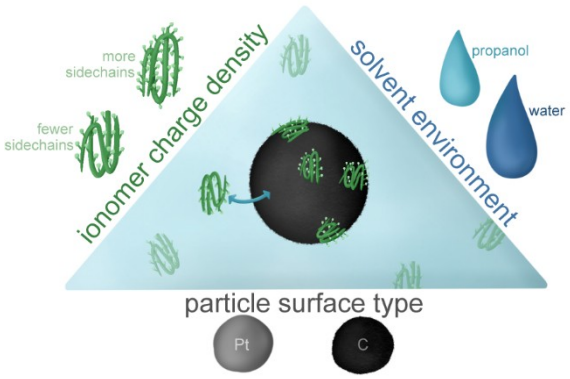

The world is increasingly focused on next-generation energy-conversion devices (e.g., fuel cells, CO_2 and water electrolyzers, *etc*.) that curtail greenhouse-gas emissions and enable a renewable, electrified economy. Key in these technologies are their catalyst layers (CLs): complex porous electrodes comprised of ion-conducting polymer (ionomer) and catalyst particle agglomerates.[1] CLs are manufactured through solution-processing techniques involving casting/drying an ink[2]: a colloidal dispersion of particles (typically platinum-on-carbon in electrolyzer cathodes or fuel cells), ionomer, and mixed solvents. The most commonly used ionomer is perfluorosulfonic acid (PFSA, structure shown in Figure S1 in the Supporting Information, SI), which has a polytetrafluoroethylene backbone and sulfonic-acid group terminated sidechains. The sidechain spacing defines the equivalent weight (EW, g polymer/mol SO_3^-).[3] Many studies have characterized dried CLs to understand structure-property-performance relationships.[4-8] However, little is known about how to direct specific structures during manufacturing, which to date has been primarily empirical and thus non predictive. Enabling next-generation CLs and designing them *a priori* necessitates understanding the forces controlling formation and structure, especially the ionomer/particle interaction.[9-10] This ink-to-CL progression is depicted in Figure 1.

Solvent identity is a critical parameter that impacts ink properties and CL microstructure. The contrasting hydrophobic backbone and hydrophilic sidechains of PFSA have competing preferences in solution, and changing solvent type (including the water:propanol ratio, two common ink solvents) causes PFSA to adopt conformations that reflect this.[11-20] (Here and throughout we mean "in solution" to mean dispersed in a solution of solvents. This does not suggest that the ionomer or nanoparticles are fully solubilized.) These different ionomer

conformations (i.e. dispersion structures) affect the self-assembly of ionomer aggregates and the properties of their films post-drying.[21-22] Furthermore, different conformations will alter how the ionomer adsorbs to catalyst particles. Changing the water:propanol ratio affects the acidity of dispersions, impacting electrostatic interactions between the ionomer and particles.[19] Atomistic molecular dynamics (MD) simulations reveal that both solvent and EW control ionomer adsorption to model carbon surfaces.[23] Additionally, there seems to be a hydrophobic interaction between the ionomer backbone and the carbon surface. The impact of solvent[4, 19, 24-28] and particle type[29-30] on ink aggregation is attributed to differences in ionomer/particle interactions, which propagate to impact the overall current-voltage behavior of the device[4, 26, 28, 31-38]. Metrics like ink zeta potential have been shown to correlate well with mass activity, non-Fickian resistance, and limiting current density and to be dependent on ink water:propanol ratios: maximum performance of each of these parameters is observed at intermediate water concentrations.[4] This can be explained by competing microstructural changes: increasing ionomer coverage of the agglomerates and increasing agglomerate size as ink water content increases.[4] Clearly, ionomer/particle agglomerates are impacted by the interactions between these components in solution. However, decoupling particle type, solvent, and EW influences on ionomer adsorption behavior remains a challenge.

In short, CL performance depends greatly on the ionomer/particle interaction. Despite the various previous investigations, fundamental questions remain regarding the specifics of this ink interaction: what is the mechanism for ionomer adsorption to particles? Does the ionomer preferentially interact with certain materials rather than others? How does the presence of different solvents alter this interaction? Answering these questions is vital toward understanding CL inks and eventual control of CL structure and performance. In this letter, we explore these

interplays by systematically measuring ionomer adsorption onto model surfaces (to understand the impact of platinum and surface hydrophobicity) with quartz-crystal microbalance (QCM) to screen adsorption as a function of solvent (water and *n*-propanol), EW, and surface type, as illustrated in Figure 1. For the majority of this study, we use 3M PFSA as a model ionomer due to the range of EWs available. To complement the QCM adsorption screening, we ascertain quantitative thermodynamic binding information (binding strength and mechanism) using isothermal titration calorimetry (ITC) on carbon and platinum nanoparticles. We conclude by discussing how other important parameters, including dispersion age and sidechain chemistry alter binding behavior.

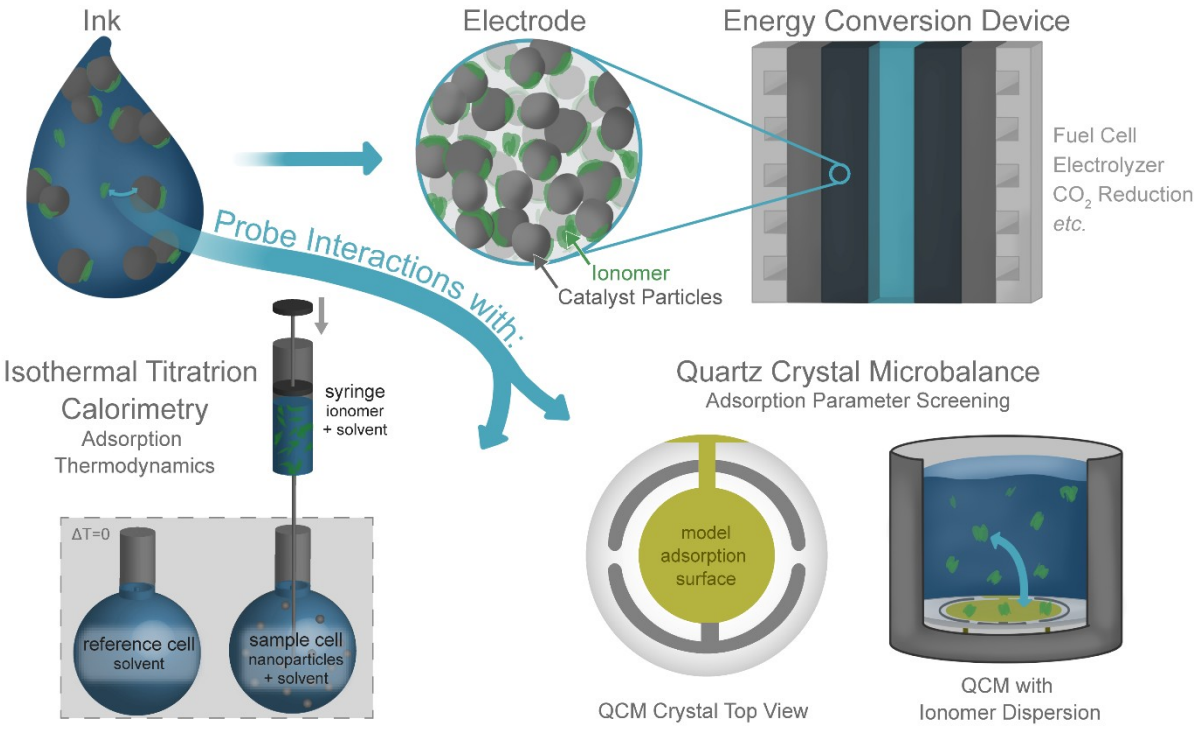

Figure 1. Ink-to-electrode progression, depicting that ionomer adsorption to catalyst particles impacts electrode structure. In this letter, we probe these interactions with both isothermal titration calorimetry

(adsorption thermodynamics) and quartz crystal microbalance (QCM, to screen the influence of solvent, surface type, and ionomer charge density parameters on adsorption) as illustrated.

Adsorption Screening. Different solvents impact how the ionomer interacts with the catalyst particles and how these ionomer/particle aggregates interact with each other. In most ink-level studies, these two effects are extremely difficult to decouple. QCM is uniquely suited to study the ionomer/particle interaction: by holding the surface constant, thereby removing the impact of solvent on particle aggregation, one can systematically investigate the impact of solvent on ionomer adsorption to a surface. By measuring the resonant frequency of the quartz crystal (Δf), one can calculate the mass change (Δm) due to adsorbed polymer from solution onto the crystal surface. The most common surfaces found in these classes of electrocatalyst nanoparticles are platinum and carbon. Therefore, we use model platinum and functionalized-gold QCM surfaces to probe the ionomer/platinum and ionomer/substrate interactions across a range of different substrate hydrophobicities (a key parameter for carbon supports): hydrophobic (alkane-thiol self-assembled monolayers, SAMs) and hydrophilic (hydroxyl- and carboxyl-terminated SAMs) functionalized gold, as well as pristine gold and platinum surfaces. The water contact angles for these surfaces increase according to alkane>carboxyl>gold>hydroxyl>platinum (Figure S2/Table S1). For each surface studied, the ionomer EW (620, 825, or 1000 g/mol SO_3^-) and the solvent used to disperse the ionomer are varied, creating a substrate/EW/solvent parameter matrix (shown in Table S1). Although the planar QCM geometry differs from the spherical aspect ratio of nanoparticles, these results elucidate the relative importance of each parameter on PFSA adsorption from solution. Experimental details of functionalization and data analysis (including frequency-signal-to-mass transformation and justification of analysis methods) are reported in

the SI. By looking at the raw data, one can determine that ionomer adsorption to these surfaces is reversible (an example is shown in Figure S3), and that adsorption kinetics for all tested conditions proceed at the same rate (Figure S6).

To explore the effect of solvent, the two EW (620 and 1000) and substrate (in terms of contact angle: alkane-thiol and platinum) extremes are used. Higher EWs indicate relatively fewer sidechains per gram of polymer, or greater sidechain spacing (more backbone tetrafluoroethylene groups). 3M 1000 has the maximum spacing (equal to Nafion explored later) of the ionomers studied. The ionomers are dispersed in various water:*n*-propanol ratios. The frequency change of the quartz crystal due to ionomer adsorption in solvent, relative to the frequency of the crystal in pure solvent, and the associated adsorbed polymer mass is plotted in Figure 2.

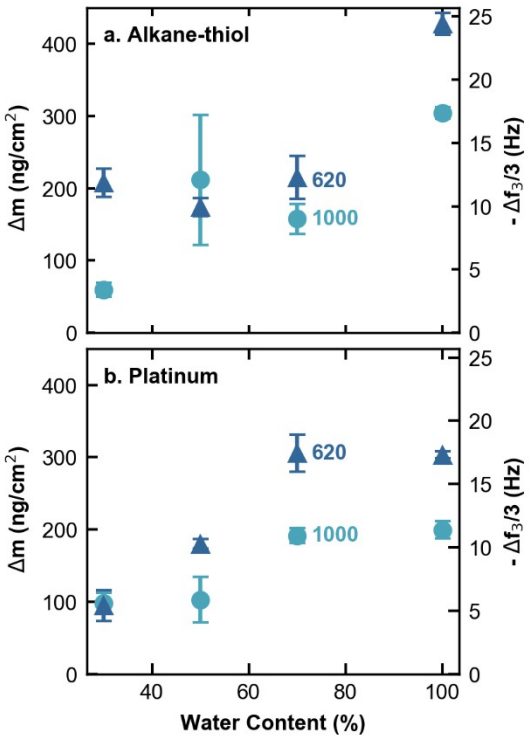

Figure 2. Frequency change (Δf) measured at the third overtone and associated mass change (Δm) due to ionomer adsorption in solution (as compared with pure solvent) on (a.) alkane-thiol and (b.) platinum

model surfaces, respectively, for ionomers with EWs of 620 and 1000 g/mol SO_3^- dispersed in a range of water:*n*-propanol ratios, reported as weight percentage water.

Adsorption depends strongly on EW and solvent, in agreement with MD simulations.[23] Increasing water content from 30% to 100% promotes ionomer adsorption, likely a result of entropic hydrophobic interactions (as discussed below and consistent with the ITC results). If the interaction between the surfaces and the ionomer is driven by hydrophobic interactions, more water in the dispersion would induce hydrophobic entities in solution to minimize their contact area with water. This would cause both more ionomer aggregation/association in the dispersion (i.e. phase partitioning of hydrophobic components), and also cause the ionomer to be less well-solubilized, driving adsorption to other surfaces (i.e. nanoparticles, the crystal surface, etc.). Because the adsorption trend holds across different surfaces types (the platinum and alkane-thiol surface), this suggests adsorption is controlled by solvent-driven interactions (i.e. hydrophobic interactions), rather than specific ionomer/surface interactions (although the magnitude of adsorption is indeed affected by surface type – and is greater on the hydrophobic alkane surface than the platinum surface). The conformation of the ionomer (as a result of ionomer/solvent interactions) also likely impacts adsorption behavior. Moving to the propanol extreme (0% water), adsorption again increases (see Figure S5). This increase is likely due to changing ionomer conformation: at the solvent extremes, the ionomer adopts a smaller, more micellar structure[12, 20], that is likely able to pack and adsorb more readily than the swollen structures at intermediate water contents.

When comparing the 30% water-content results to the >80% water-content, 3M 1000 adsorbs roughly 200% more onto platinum surfaces and 3M 620 adsorbs about 300% more. These values

correspond to ~20% coverage on the crystal at low-water contents to near-complete coverage at high-water contents (coverage estimates discussed in the SI). A similar trend has been observed by AFM studies: more ionomer aggregates adsorb on platinum at higher water concentrations.[39] These differences are significant and dictate the amount of ionomer strongly interacting with catalyst particle surfaces versus free in solution, the latter of which likely leads to large ionomer agglomerates upon drying and CL formation. Therefore, tuning the water:alcohol ratio directs how much ionomer adsorbs to particles, thereby controlling CL morphology/performance[4, 28].

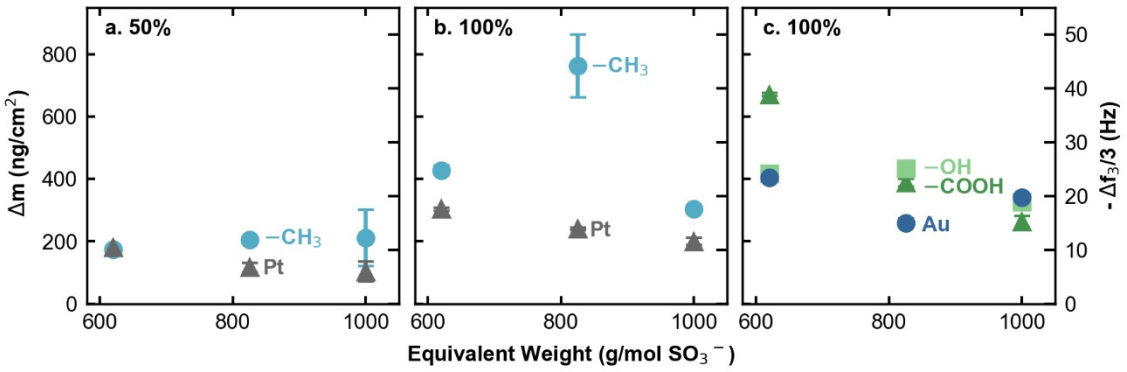

Figure 3. Frequency change (Δf) measured at the third overtone and associated mass change (Δm) due to ionomer adsorption in solution (as compared with pure solvent) for a range of EWs on surfaces with alkane (-CH_3), platinum (Pt), gold (Au), hydroxyl (-OH), and carboxyl (-COOH) functionality in (a.) 50:50 (wt%) water:*n*-propanol and (b.,c.) 100% water.

Figure 3 examines the relationship between EW and surface type. By comparing Figure 3a with 3b, it is evident for all EW that more ionomer adsorbs to alkane-thiol and platinum surfaces in 100% water than in 50:50 (wt%) water:*n*-propanol (see Figure 2). In both solvent mixtures, as EW decreases, ionomer adsorption to platinum increases. This same trend is observed for the other hydrophilic surfaces studied in Figure 3c. Importantly, PFSA adsorption to platinum

represents the lowest adsorption magnitude among the surfaces studied (in agreement with other studies that showed the PFSA/platinum interaction was weaker than the PFSA/gold interaction[40-41]). Some hypothesize that there is a strong specific interaction between PFSA sulfonate groups and platinum, and that this interaction drives PFSA adsorption to catalyst particles in inks. However, we do not see indications of this (due to low adsorption), counter to other experimental evidence that shows sulfonate adsorption to platinum surfaces[40, 42-44]. This is rationalized because the platinum in those experiments was polarized (relative to the potential of zero charge[45-48]), while ours is under no applied potential. Additionally, in the *operando* PFSA/platinum interaction studies, the platinum is likely in a metallic state; conversely, the platinum surfaces here (and found in inks) will have some native oxide coverage, which has been shown to impact PFSA behavior.[49] Therefore, the PFSA/platinum interaction in solution versus in operating CLs is different, likely due to different surface charge states. An explanation as to why PFSA adsorption increases with decreasing EW could be that as the ionomer becomes more hydrophilic (as shown by increased acidity[19-20]), it can more readily interact with platinum; scattering studies show PFSA backbone chains orient on hydrophobic surfaces differently than they do on hydrophilic ones[50-51]. The PFSA/platinum interaction will be discussed further below.

Based on the platinum adsorption trend, one might expect the opposite trend for the hydrophobic surface: as ionomer EW increases, so would adsorption. This is seen weakly in the 50% solvent environment, but the trend very obviously deviates for 100% water. In the 50% solvent, the ionomer has a loose, lamellar structure (given phase diagram dielectric constant predictions[20]), in contrast with the tight, condensed rods observed at higher water contents.[12, 19-20] This loose structure could result in high sidechain mobility, allowing for adsorption to scale with EW in a more linear manner than at higher water contents. With more collapsed conformations

in pure water,[11, 19] it is reasonable to expect different trends. While additional solution structure data is needed to confirm this, it is possible that 3M 825 possesses an appropriate ratio of hydrophilic and hydrophobic moieties such that its conformation in water is optimal for adsorption to hydrophobic surfaces; ITC data presented in the next section confirms that 3M 825 also possesses the strongest binding constant among the ionomers studied to hydrophobic surfaces. Indeed, this may be consistent with the fact that 3M 825 is 3M's commercial dispersion for fuel cells. Additional reasons for the nonlinear EW trend could be due to differences in molecular weight[52] between the ionomers. However, because the trends change as a function of surface type and solvent, and because the molecular weights are so large (~250 kDa), we expect molecular weight effects to be secondary to the impact of EW. Of note, it is possible that in highly concentrated polymer regimes, these effects may have more influence.[53-54]

Thermodynamics of Binding. To gain quantitative thermodynamic binding information and delineate the ionomer/particle interactions, ITC is performed with the various ionomers and platinum or Vulcan-carbon nanoparticles, where the latter is typically used in CLs and, as will be shown, is approximated by alkane-thiol SAMs in the QCM experiments. The ionomer dispersions are titrated into a sample cell containing nanoparticles (in pure water); the power required to keep the cell at a constant temperature is monitored. By integrating the power over time, adsorption heats and binding isotherms are measured. The data shown here are parameters (association constant, K_A, adsorption enthalpy and entropy) extracted from an independent (Langmuir) binding model fit with appropriate subtraction to remove heats of mixing/dilution (see SI for example raw data and model fits). Both freshly prepared dispersions (like those used

in the QCM experiments) and aged dispersions (prepared two weeks prior and remixed before using) are studied.

Figure 4 shows K_A for the three EWs on Vulcan carbon and platinum-black nanoparticles. Because the binding constants are on a gram basis, one should not compare values across different particle types (they will have a different number of binding sites per gram, molar data is presented in Figure S9). We first consider the new dispersion data. Notably, the EW trends on carbon and platinum are the same as those observed in the QCM experiments (Figure 3b): weaker binding is observed on platinum as EW increases, and binding to carbon has the same nonlinear EW dependence; the alkane-thiol surface is therefore a good proxy for Vulcan.

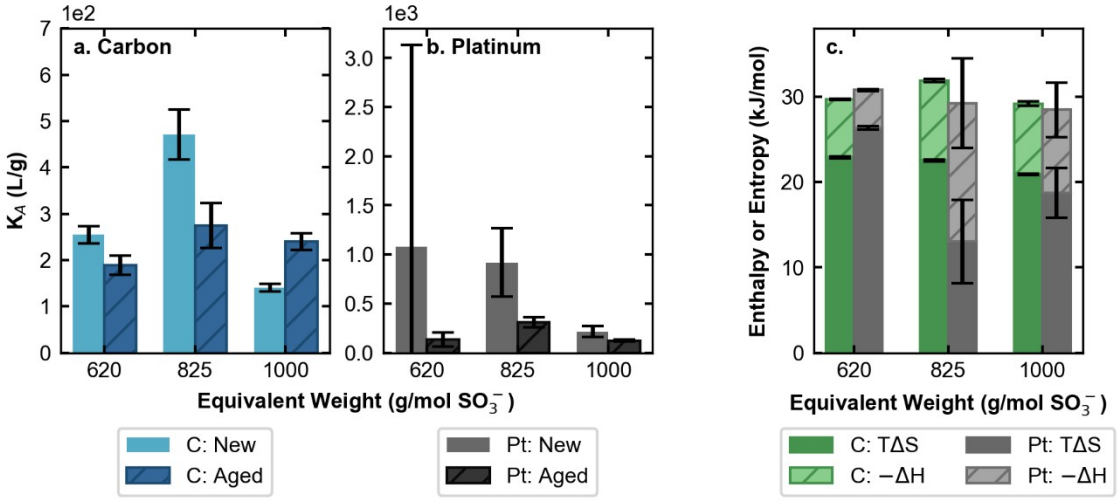

Figure 4. Association constants (K_A) of ionomer binding to (a.) carbon or (b.) platinum nanoparticles for freshly prepared (New) or older (Aged) dispersions as a function of ionomer EW in water. Note quantitative comparisons should not be made between (a.) and (b.) because K_A is on a gram basis. (c.) Stacked plot displaying the absolute value of the enthalpic and entropic contributions to the positive binding free energy for the New dispersions (all values indicate spontaneous adsorption).

The enthalpic (-ΔH) and entropic (TΔS) contribution to the positive free energy ($|\Delta G| = RT\ln[K_A]$) for PFSA binding is plotted in Figure 4c. Energy values are in agreement with those

calculated for other ionomer isotherms,[55] and are similar or weaker than those observed for protein/surface interactions,[56-58] although quantitative values depend on molar-conversion assumptions (see SI). Immediately evident is that the entropic contribution is larger than the enthalpic contribution, regardless of EW or particle identity. Enthalpic signatures are representative of specific-binding, hydrogen bonding, *etc*., while spontaneous entropically-driven binding in aqueous solutions is often due to hydrophobic interactions.[56, 58] These entropic hydrophobic interactions arise (at small distances) because liberated water molecules (excluded solvent) gain entropy when surfaces come together, offsetting the loss in conformational entropy of the adsorbate. This entropically-driven ITC data is consistent with previous MD[23, 27, 30] and experimental[59] results that conclude adsorption to carbon surfaces is driven by hydrophobic interactions with the backbone. Interestingly, PFSA adsorption to platinum is also entropically-dominated, suggesting specific-binding between sulfonate and platinum (which would manifest as an enthalpic ITC signature) is not the primary ionomer/platinum interaction under these (non-polarized) conditions. This agrees with one study that noted the co-adsorption of fluorocarbon groups in addition to sulfonate at elevated potentials.[40] These results indicate that the ionomer/platinum interaction is not especially strong (at least compared to the ionomer/carbon interaction) in inks, and that adsorption to platinum is controlled by a similar mechanism as to carbon.

Therefore, given the larger surface area of carbon relative to platinum in most electrocatalyst particles, PFSA/particle adsorption (and subsequent aggregation) in inks is likely dominated by the PFSA/carbon interaction. Indeed, carbon treatment methods to tune the PFSA/carbon interaction have been successfully employed to control CL performance.[60-61] Similarly, one metric often reported is the ionomer-to-carbon (I/C) ratio, where optimal ratios[62-68] seem

dependent on carbon type; given the results herein, ideal ratios will also likely vary with solvent and EW.

Additional Parameters. Another consideration is how these PFSA/particle interactions vary with time. If the binding behavior of these dispersions is measured two weeks later, the interaction strength and trends change, as seen for the aged data in Figure 4. Generally, the interaction becomes weaker with time. However, the binding mechanism remains entropically driven (in fact, even more so, Figure S10). PFSA conformational changes are evidenced by the significant change in dispersion pH[19] as a function of time (Figure S11). This suggests that there is a slow equilibrium timescale for reorganization when these dispersions are prepared, and that they maintain some memory of their previous state (considering that pH changes are greater the more dissimilar the dispersion solvent is from its initial solvent). Additional factors that could influence dispersion conformation over time could result from radical formation during sonication[69], although this is unlikely given the sonication power used here. These time-dependent results have critical implications for CLs cast from inks of different age, and may help explain changes in CL microstructure and performance.[70]

Finally, it is of interest to understand the role sidechain length and chemistry play on these interactions. To examine this, Figure 5 compares Nafion 1100 and 3M 1000 as they have same sidechain spacing but Nafion has a longer sidechain with an extra ether oxygen (see Figure S1). Within error, binding of these two ionomers to both particle types and adsorption to both QCM surfaces is the same. This indicates that EW is a stronger predictor of binding affinity than sidechain length, in agreement with model thin-film[71] and CL studies.[72]

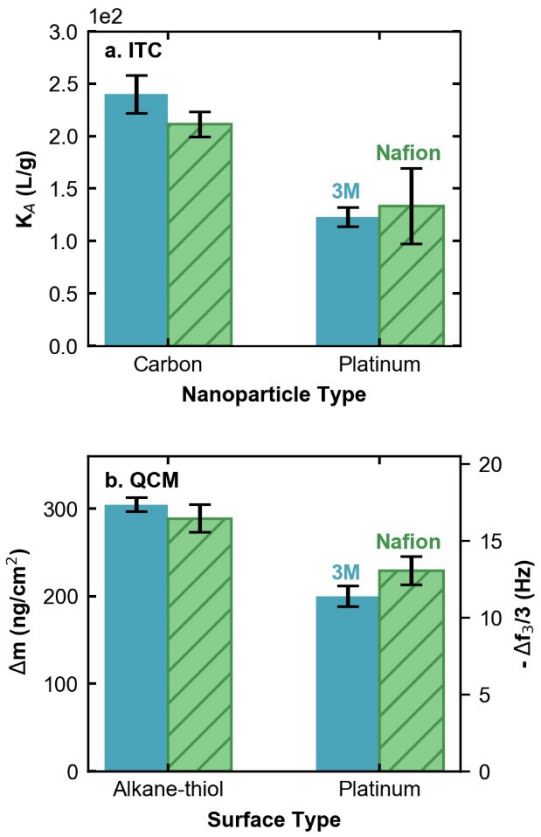

Figure 5. (a.) Association constants (K_A) of 3M 1000 versus Nafion 1100 binding on carbon and platinum black nanoparticles from ITC measurements. (b.) Frequency change (Δf) measured at the third overtone and associated mass change (Δm) due to ionomer adsorption (3M 1000 or Nafion 1100) in 100% water onto alkane-thiol-modified and platinum QCM surfaces.

In summary, we used both QCM and ITC data to understand the influence of solvent environment, EW, surface type, and sidechain length on PFSA adsorption. PFSA adsorption strongly depends on solvent environment: as the water:propanol ratio increases from intermediate water concentrations to high water concentrations, PFSA adsorption increases regardless of surface type, suggesting both that hydrophobic partitioning and ionomer conformation drive adsorption in water/alcohol solvents. When holding solvent constant, adsorption depends on EW and surface type. Interestingly, ITC data suggests the binding

mechanism to platinum versus carbon is similar (entropic/hydrophobically driven). Given this, and considering that adsorption from ink-relevant solvents is lower on platinum versus hydrophobic QCM surfaces, it is likely that ionomer/particle aggregation in inks is dominated by ionomer/carbon rather than ionomer/platinum interactions, especially when considering the larger carbon surface area relative to platinum in many platinum-on-carbon nanoparticles. This is contrary to the hypothesis that sulfonate group/platinum interactions control ink adsorption. While these sulfonate interactions dominate in operating devices, the QCM and ITC data presented herein suggest these interactions are not controlling in ink systems, where surface charge states of platinum are different. Importantly, these ink interactions will control agglomerate microstructure formation, and thus will also control the amount of ionomer (and sulfonate groups) available to interact with the platinum surface once under applied potential. While additional work is needed to understand more completely how dispersions change with time, these ionomer/particle interactions are dynamic and have the potential to significantly influence ink aggregate structures (and eventual CL structures/interfaces).

The complex surface/EW/solvent parameter space explored in this letter controls the forces between ink constituents and determines the CL microstructure upon drying; thus, the data presented herein is critical in unraveling the governing interactions and phenomena. More importantly, with this new understanding we can now engineer inks to promote (or demote) adsorption to specific surfaces in order to control optimal CL performance and electrode designs for many energy-conversion technologies.

ASSOCIATED CONTENT

Supporting Information. Details of experimental methods, including raw data and analysis for QCM and ITC, surface functionalization, adsorption kinetics, molar conversions, aging data (pH, enthalpy/entropy)

ACKNOWLEDGEMENTS

The authors would like to thank Dr. Behzad Rad, Professor Clayton Radke, Dr. Andrew Crothers, Ms. Rebecca Pinals, Ms. Anamika Chowdhury, and Dr. Peter Dudenas for helpful discussions. We would also like to thank Dr. Douglas Kushner for assistance with designing the QCM-crystal functionalization holder. This material is primarily based on work performed by the Million Mile Fuel Cell Truck (M^2FCT) Consortium (https://millionmilefuelcelltruck.org), technology manager Greg Kleen, which is supported by the U.S. Department of Energy, Office of Energy Efficiency and Renewable Energy, Hydrogen and Fuel Cell Technologies Office, under contract number DE-AC02-05CH1123, with initial funding from the Fuel Cell Performance and Durability Consortium (FC-PAD). ITC work conducted at the Molecular Foundry was supported by the Office of Science, Office of Basic Energy Sciences, of the U.S. Department of Energy under Contract No. DE-AC02-05CH11231. S.A.B acknowledges support from the Graduate Research Fellowship Program by the National Science Foundation under Grant No. DGE 1752814.

REFERENCES

1. Holdcroft, S., Fuel Cell Catalyst Layers: A Polymer Science Perspective. *Chem. Mater.* **2014,** *26* (1), 381-393.
2. Hatzell, K. B.; Dixit, M. B.; Berlinger, S. A.; Weber, A. Z., Understanding inks for porous-electrode formation. *J. Mater. Chem. A* **2017,** *5* (39), 20527-20533.
3. Kusoglu, A.; Weber, A. Z., New Insights into Perfluorinated Sulfonic-Acid Ionomers. *Chem. Rev.* **2017,** *117* (3), 987-1104.
4. Van Cleve, T.; Khandavalli, S.; Chowdhury, A.; Medina, S.; Pylypenko, S.; Wang, M.; More, K. L.; Kariuki, N.; Myers, D. J.; Weber, A. Z.; Mauger, S. A.; Ulsh, M.; Neyerlin, K. C., Dictating Pt-Based Electrocatalyst Performance in Polymer Electrolyte Fuel Cells, from Formulation to Application. *ACS Appl. Mater. Interfaces* **2019,** *11* (50), 46953-46964.
5. Cetinbas, F. C.; Ahluwalia, R. K.; Kariuki, N. N.; Myers, D. J., Agglomerates in Polymer Electrolyte Fuel Cell Electrodes: Part I. Structural Characterization. *J. Electrochem. Soc.* **2018,** *165* (13), F1051-F1058.
6. Epting, W. K.; Gelb, J.; Litster, S., Resolving the Three-Dimensional Microstructure of Polymer Electrolyte Fuel Cell Electrodes using Nanometer-Scale X-ray Computed Tomography. *Advanced Functional Materials* **2012,** *22* (3), 555-560.
7. Cullen, D. A.; Koestner, R.; Kukreja, R. S.; Liu, Z. Y.; Minko, S.; Trotsenko, O.; Tokarev, A.; Guetaz, L.; Meyer, H. M.; Parish, C. M.; More, K. L., Imaging and Microanalysis of Thin Ionomer Layers by Scanning Transmission Electron Microscopy. *J. Electrochem. Soc.* **2014,** *161* (10), F1111-F1117.
8. Lei, C.; Fan, Y.; Natalia, M.; Magali, S.; Geraldine, M. P.; Jasna, J.; David, C.; Karren, L. M.; Yu Seung, K.; Hui, X., Impact of Catalyst Ink Dispersing Solvent on PEM Fuel Cell Performance and Durability. *J. Electrochem. Soc.* **2021,** *168*, 044517.
9. Woo, S.; Lee, S.; Taning, A. Z.; Yang, T.-H.; Park, S.-H.; Yim, S.-D., Current understanding of catalyst/ionomer interfacial structure and phenomena affecting the oxygen reduction reaction in cathode catalyst layers of proton exchange membrane fuel cells. *Current Opinion in Electrochemistry* **2020,** *21*, 289-296.
10. Berlinger, S. A.; Garg, S.; Weber, A. Z., Multicomponent, multiphase interactions in fuel-cell inks. *Current Opinion in Electrochemistry* **2021,** *29*, 100744.
11. Gebel, G.; Loppinet, B., Colloidal structure of ionomer solutions in polar solvents. *J. Mol. Struct.* **1996,** *383* (1), 43-49.
12. Welch, C.; Labouriau, A.; Hjelm, R.; Orler, B.; Johnston, C.; Kim, Y. S., Nafion in Dilute Solvent Systems: Dispersion or Solution? *ACS Macro. Lett.* **2012,** *1* (12), 1403-1407.
13. Lee, S.-J.; Yu, T. L.; Lin, H.-L.; Liu, W.-H.; Lai, C.-L., Solution properties of nafion in methanol/water mixture solvent. *Polymer* **2004,** *45* (8), 2853-2862.
14. Aldebert, P.; Gebel, G.; Loppinet, B.; Nakamura, N., Polyelectrolyte effect in perfluorosulfonated ionomer solutions. *Polymer* **1995,** *36* (2), 431-434.
15. Loppinet, B.; Gebel, G.; Williams, C. E., Small-Angle Scattering Study of Perfluorosulfonated Ionomer Solutions. *J. Phys. Chem. B.* **1997,** *101* (10), 1884-1892.
16. Loppinet, B.; Gebel, G., Rodlike Colloidal Structure of Short Pendant Chain Perfluorinated Ionomer Solutions. *Langmuir* **1998,** *14* (8), 1977-1983.
17. Mabuchi, T.; Huang, S.-F.; Tokumasu, T., Nafion Ionomer Dispersion in Mixtures of 1-Propanol and Water Based on the Martini Coarse-Grained Model. *Journal of Polymer Science* **2020,** *58* (3), 487-499.
18. Mabuchi, T.; Huang, S.-F.; Tokumasu, T., Dispersion of Nafion Ionomer Aggregates in 1-Propanol/Water Solutions: Effects of Ionomer Concentration, Alcohol Content, and Salt Addition. *Macromolecules* **2020,** *53* (9), 3273-3283.
19. Berlinger, S. A.; McCloskey, B. D.; Weber, A. Z., Inherent Acidity of Perfluorosulfonic Acid Ionomer Dispersions and Implications for Ink Aggregation. *J. Phys. Chem. B.* **2018,** *122* (31), 7790-7796.
20. Tarokh, A.; Karan, K.; Ponnurangam, S., Atomistic MD Study of Nafion Dispersions: Role of Solvent and Counterion in the Aggregate Structure, Ionic Clustering, and Acid Dissociation. *Macromolecules* **2020,** *53* (1), 288-301.

21. Berlinger, S. A.; Dudenas, P. J.; Bird, A.; Chen, X.; Freychet, G.; McCloskey, B. D.; Kusoglu, A.; Weber, A. Z., Impact of Dispersion Solvent on Ionomer Thin Films and Membranes. *ACS Applied Polymer Materials* **2020,** *2* (12), 5824-5834.
22. Dudenas, P. J.; Kusoglu, A., Evolution of Ionomer Morphology from Dispersion to Film: An in Situ X-ray Study. *Macromolecules* **2019,** *52* (20), 7779-7785.
23. Mashio, T.; Ohma, A.; Tokumasu, T., Molecular Dynamics Study of Ionomer Adsorption at a Carbon Surface in Catalyst Ink. *Electrochim. Acta* **2016,** *202*, 14-23.
24. Dixit, M. B.; Harkey, B. A.; Shen, F.; Hatzell, K. B., Catalyst Layer Ink Interactions That Affect Coatability. *J. Electrochem. Soc.* **2018,** *165* (5), F264-F271.
25. Shukla, S.; Bhattacharjee, S.; Weber, A. Z.; Secanell, M., Experimental and Theoretical Analysis of Ink Dispersion Stability for Polymer Electrolyte Fuel Cell Applications. *J. Electrochem. Soc.* **2017,** *164* (6), F600-F609.
26. Orfanidi, A.; Rheinländer, P. J.; Schulte, N.; Gasteiger, H. A., Ink Solvent Dependence of the Ionomer Distribution in the Catalyst Layer of a PEMFC. *J. Electrochem. Soc.* **2018,** *165* (14), F1254-F1263.
27. Malek, K.; Eikerling, M.; Wang, Q.; Navessin, T.; Liu, Z., Self-Organization in Catalyst Layers of Polymer Electrolyte Fuel Cells. *J. Phys. Chem. C.* **2007,** *111* (36), 13627-13634.
28. Van Cleve, T.; Wang, G.; Mooney, M.; Cetinbas, C. F.; Kariuki, N.; Park, J.; Farghaly, A.; Myers, D.; Neyerlin, K. C., Tailoring electrode microstructure via ink content to enable improved rated power performance for platinum cobalt/high surface area carbon based polymer electrolyte fuel cells. *J. Power Sources* **2021,** *482*, 228889.
29. Khandavalli, S.; Park, J. H.; Kariuki, N. N.; Myers, D. J.; Stickel, J. J.; Hurst, K.; Neyerlin, K. C.; Ulsh, M.; Mauger, S. A., Rheological Investigation on the Microstructure of Fuel Cell Catalyst Inks. *ACS Appl. Mater. Interfaces* **2018,** *10* (50), 43610-43622.
30. Mashio, T.; Malek, K.; Eikerling, M.; Ohma, A.; Kanesaka, H.; Shinohara, K., Molecular Dynamics Study of Ionomer and Water Adsorption at Carbon Support Materials. *J. Phys. Chem. C.* **2010,** *114* (32), 13739-13745.
31. Shin, S. J.; Lee, J. K.; Ha, H. Y.; Hong, S. A.; Chun, H. S.; Oh, I. H., Effect of the catalytic ink preparation method on the performance of polymer electrolyte membrane fuel cells. *J. Power Sources* **2002,** *106* (1–2), 146-152.
32. Xie, Z.; Navessin, T.; Zhao, X.; Adachi, M.; Holdcroft, S.; Mashio, T.; Ohma, A.; Shinohara, K., Nafion Ionomer Aggregation and its Influence on Proton Conduction and Mass Transport in Fuel Cell Catalyst Layers. *ECS Trans.* **2008,** *16* (2), 1811-1816.
33. Ngo, T. T.; Yu, T. L.; Lin, H.-L., Influence of the composition of isopropyl alcohol/water mixture solvents in catalyst ink solutions on proton exchange membrane fuel cell performance. *J. Power Sources* **2013,** *225*, 293-303.
34. Uchida, M.; Aoyama, Y.; Eda, N.; Ohta, A., New Preparation Method for Polymer-Electrolyte Fuel Cells. *J. Electrochem. Soc.* **1995,** *142* (2), 463-468.
35. Huang, D. C.; Yu, P. J.; Liu, F. J.; Huang, S. L.; Hsueh, K. L.; Chen, Y. C.; Wu, C. H.; Chang, W. C.; Tsau, F. H., Effect of Dispersion Solvent in Catalyst Ink on Proton Exchange Membrane Fuel Cell Performance. *Int. J. Electrochem. Sci.* **2011,** *6* (7), 2551-2565.
36. Johnston, C. M.; Lee, K.-S.; Rockward, T.; Labouriau, A.; Mack, N.; Kim, Y. S., Impact of Solvent on Ionomer Structure and Fuel Cell Durability. *ECS Trans.* **2009,** *25* (1), 1617-1622.
37. Therdthianwong, A.; Ekdharmasuit, P.; Therdthianwong, S., Fabrication and Performance of Membrane Electrode Assembly Prepared by a Catalyst-Coated Membrane Method: Effect of Solvents Used in a Catalyst Ink Mixture. *Energy Fuels* **2010,** *24* (2), 1191-1196.
38. Kim, T.-H.; Yi, J.-Y.; Jung, C.-Y.; Jeong, E.; Yi, S.-C., Solvent effect on the Nafion agglomerate morphology in the catalyst layer of the proton exchange membrane fuel cells. *Int. J. Hydrogen Energy* **2017,** *42* (1), 478-485.
39. Devivaraprasad, R.; Masuda, T., Solvent-Dependent Adsorption of Perfluorosulfonated Ionomers on a Pt(111) Surface Using Atomic Force Microscopy. *Langmuir* **2020,** *36* (46), 13793-13798.

40. Masuda, T.; Sonsudin, F.; Singh, P. R.; Naohara, H.; Uosaki, K., Potential-Dependent Adsorption and Desorption of Perfluorosulfonated Ionomer on a Platinum Electrode Surface Probed by Electrochemical Quartz Crystal Microbalance and Atomic Force Microscopy. *J. Phys. Chem. C.* **2013,** *117* (30), 15704-15709.
41. Masuda, T.; Ikeda, K.; Uosaki, K., Potential-Dependent Adsorption/Desorption Behavior of Perfluorosulfonated Ionomer on a Gold Electrode Surface Studied by Cyclic Voltammetry, Electrochemical Quartz Microbalance, and Electrochemical Atomic Force Microscopy. *Langmuir* **2013,** *29* (7), 2420-2426.
42. Subbaraman, R.; Strmcnik, D.; Stamenkovic, V.; Markovic, N. M., Three Phase Interfaces at Electrified Metal−Solid Electrolyte Systems 1. Study of the Pt(hkl)−Nafion Interface. *J. Phys. Chem. C.* **2010,** *114* (18), 8414-8422.
43. Kendrick, I.; Kumari, D.; Yakaboski, A.; Dimakis, N.; Smotkin, E. S., Elucidating the Ionomer-Electrified Metal Interface. *Journal of the American Chemical Society* **2010,** *132* (49), 17611-17616.
44. Koestner, R.; Roiter, Y.; Kozhinova, I.; Minko, S., Effect of Local Charge Distribution on Graphite Surface on Nafion Polymer Adsorption as Visualized at the Molecular Level. *J. Phys. Chem. C.* **2011,** *115* (32), 16019-16026.
45. Muzaffar, T.; Kadyk, T.; Eikerling, M., Physical Modeling of the Proton Density in Nanopores of PEM Fuel Cell Catalyst Layers. *Electrochim. Acta* **2017,** *245*, 1048-1058.
46. Garrick, T. R.; Moylan, T. E.; Yarlagadda, V.; Kongkanand, A., Characterizing Electrolyte and Platinum Interface in PEM Fuel Cells Using CO Displacement. *J. Electrochem. Soc.* **2016,** *164* (2), F60-F64.
47. Huang, J.; Malek, A.; Zhang, J.; Eikerling, M. H., Non-monotonic Surface Charging Behavior of Platinum: A Paradigm Change. *J. Phys. Chem. C.* **2016,** *120* (25), 13587-13595.
48. Zenyuk, I. V.; Litster, S., Modeling ion conduction and electrochemical reactions in water films on thin-film metal electrodes with application to low temperature fuel cells. *Electrochim. Acta* **2014,** *146*, 194-206.
49. Tesfaye, M.; MacDonald, A. N.; Dudenas, P. J.; Kusoglu, A.; Weber, A. Z., Exploring substrate/ionomer interaction under oxidizing and reducing environments. *Electrochemistry Communications* **2018,** *87*, 86-90.
50. Modestino, M. A.; Kusoglu, A.; Hexemer, A.; Weber, A. Z.; Segalman, R. A., Controlling Nafion Structure and Properties via Wetting Interactions. *Macromolecules* **2012,** *45* (11), 4681-4688.
51. Karan, K., Interesting Facets of Surface, Interfacial, and Bulk Characteristics of Perfluorinated Ionomer Films. *Langmuir* **2019,** *35* (42), 13489-13520.
52. Nagappan, R.; Swami, K.; Roland, K.; Timothy, F.; Wenbin, G.; Nancy, N. K.; Deborah, J. M.; Peter, J. D.; Ahmet, K., Editors' Choice—Ionomer Side Chain Length and Equivalent Weight Impact on High Current Density Transport Resistances in PEMFC Cathodes. *J. Electrochem. Soc.* **2021,** *168*, 024518.
53. Janardhan, R.; Gedam, P. H.; Sampathkumaran, P. S., The effect of polymer molecular weight in the adsorption process. *J. Colloid Interface Sci.* **1990,** *140* (2), 391-400.
54. De Gennes, P., Scaling theory of polymer adsorption. *J. Phys. France* **1976,** *32* (12), 1445-1452.
55. Thoma, M.; Lin, W.; Hoffmann, E.; Sattes, M.; Segets, D.; Damm, C.; Peukert, W., A simple and reliable method for studying the adsorption behavior of Aquivion® ionomers on carbon black surfaces. *Langmuir* **2018,** *34* (41), 12324–12334.
56. Norde, W., ENERGY AND ENTROPY OF PROTEIN ADSORPTION. *Journal of Dispersion Science and Technology* **1992,** *13* (4), 363-377.
57. Johnson, R. D.; Arnold, F. H., The temkin isotherm describes heterogeneous protein adsorption. *Biochimica et Biophysica Acta (BBA) - Protein Structure and Molecular Enzymology* **1995,** *1247* (2), 293-297.
58. Prozeller, D.; Morsbach, S.; Landfester, K., Isothermal titration calorimetry as a complementary method for investigating nanoparticle–protein interactions. *Nanoscale* **2019,** *11* (41), 19265-19273.

59. Takuya, M.; Hideo, N.; Satoru, T.; R., S. P.; Kohei, U., Formation and Structure of Perfluorosulfonated Ionomer Thin Film on a Graphite Surface. *Chem. Lett.* **2009,** *38* (9), 884-885.
60. Pramounmat, N.; Loney, C. N.; Kim, C.; Wiles, L.; Ayers, K. E.; Kusoglu, A.; Renner, J. N., Controlling the Distribution of Perfluorinated Sulfonic Acid Ionomer with Elastin-like Polypeptide. *ACS Appl. Mater. Interfaces* **2019,** *11* (46), 43649–43658.
61. Orfanidi, A.; Madkikar, P.; El-Sayed, H. A.; Harzer, G. S.; Kratky, T.; Gasteiger, H. A., The Key to High Performance Low Pt Loaded Electrodes. *J. Electrochem. Soc.* **2017,** *164* (4), F418-F426.
62. Passalacqua, E.; Lufrano, F.; Squadrito, G.; Patti, A.; Giorgi, L., Nafion content in the catalyst layer of polymer electrolyte fuel cells: effects on structure and performance. *Electrochim. Acta* **2001,** *46* (6), 799-805.
63. Antolini, E.; Giorgi, L.; Pozio, A.; Passalacqua, E., Influence of Nafion loading in the catalyst layer of gas-diffusion electrodes for PEFC. *J. Power Sources* **1999,** *77* (2), 136-142.
64. Sasikumar, G.; Ihm, J. W.; Ryu, H., Optimum Nafion content in PEM fuel cell electrodes. *Electrochim. Acta* **2004,** *50* (2–3), 601-605.
65. Zhao, X.; Li, W.; Fu, Y.; Manthiram, A., Influence of ionomer content on the proton conduction and oxygen transport in the carbon-supported catalyst layers in DMFC. *Int. J. Hydrogen Energy* **2012,** *37* (12), 9845-9852.
66. Ishikawa, H.; Sugawara, Y.; Inoue, G.; Kawase, M., Effects of Pt and ionomer ratios on the structure of catalyst layer: A theoretical model for polymer electrolyte fuel cells. *J. Power Sources* **2018,** *374*, 196-204.
67. Alink, R.; Singh, R.; Schneider, P.; Christmann, K.; Schall, J.; Keding, R.; Zamel, N., Full Parametric Study of the Influence of Ionomer Content, Catalyst Loading and Catalyst Type on Oxygen and Ion Transport in PEM Fuel Cell Catalyst Layers. *Molecules* **2020,** *25* (7), 1523.
68. Schuler, T.; Chowdhury, A.; Freiberg, A. T.; Sneed, B.; Spingler, F. B.; Tucker, M. C.; More, K. L.; Radke, C. J.; Weber, A. Z., Fuel-Cell Catalyst-Layer Resistance via Hydrogen Limiting-Current Measurements. *J. Electrochem. Soc.* **2019,** *166* (7), F3020-F3031.
69. Pollet, B. G., Let's Not Ignore the Ultrasonic Effects on the Preparation of Fuel Cell Materials. *Electrocatalysis* **2014,** *5* (4), 330-343.
70. Uemura, S.; Yoshida, T.; Koga, M.; Matsumoto, H.; Yang, X.; Shinohara, K.; Sasabe, T.; Hirai, S., Ink Degradation and Its Effects on the Crack Formation of Fuel Cell Catalyst Layers. *J. Electrochem. Soc.* **2019,** *166* (2), F89-F92.
71. Kusoglu, A.; Dursch, T. J.; Weber, A. Z., Nanostructure/Swelling Relationships of Bulk and Thin-Film PFSA Ionomers. *Advanced Functional Materials* **2016,** *26* (27), 4961-4975.
72. Nagappan, R.; Swami, K.; Roland, K.; Timothy, F.; Wenbin, G.; Nancy, N. K.; Deborah, J. M.; Peter, J. D.; Ahmet, K., Editors' Choice—Ionomer Side Chain Length and Equivalent Weight Impact on High Current Density Transport Resistances in PEMFC Cathodes. *J. Electrochem. Soc.* **2021**.